

pubs.acs.org/cm Article

# Accessing High-Power Near-Infrared Spectroscopy Using Cr<sup>3+</sup>-Substituted Metal Phosphate Phosphors

Jiyou Zhong, Chaojie Li, Weiren Zhao,\* Shihai You, and Jakoah Brgoch\*



Cite This: Chem. Mater. 2022, 34, 337-344



**Read Online** 

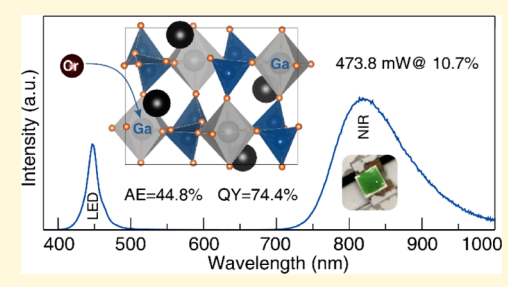
**ACCESS** 

Metrics & More



SI Supporting Information

ABSTRACT: Near-infrared (NIR) phosphor-converted light-emitting diode (pc-LED) technology has attracted considerable interest as a next-generation light source for emerging NIR spectroscopic applications. However, discovering efficient broadband NIR phosphors necessary to access the desired long-wavelength ( $\lambda_{\rm em} \geq 800$  nm) energy window remains a challenge. Here, a new phosphate phosphor, KGaP<sub>2</sub>O<sub>7</sub>:Cr<sup>3+</sup>, emerged from a fundamental study of the AMP<sub>2</sub>O<sub>7</sub> (A = Li, Na, K; M = Al, Ga, Sc, In) family. This material combines all of the requisite properties for the efficient generation of NIR photons, including limited defect formation, minimal electron—phonon coupling, a subtle octahedral site distortion, and well-separated transition metal substitution sites. Photo-



luminescence spectroscopy indicates that this material emits from 700 to 1100 nm ( $\lambda_{max} = 815$  nm) with a full width at half-maximum (fwhm) of 127 nm or 1874 cm<sup>-1</sup>. Exciting the material with a blue LED reveals a quantum yield of 74.4% with an absorption efficiency of 44.8%, resulting in an excellent external quantum efficiency as high as 33.3% from the as-prepared sample. A prototype NIR pc-LED device generated an output power of 473.8 mW and a high photoelectric conversion efficiency (10.7% under 500 mA), demonstrating the potential of applying this phosphor in blue LED-based NIR spectroscopy.

# 1. INTRODUCTION

Broadband near-infrared (NIR) light sources have attracted increased interest due to the array of applications using this energy region, including optical communication, non-destructive food analysis, plant growth, environmental monitoring, and biomedical imaging. Currently, phosphor-converted NIR light-emitting diode (pc-NIR-LED) technology is considered the best approach for NIR light generation due to their superior operating lifetimes, compact size, and low energy consumption compared to classic broadband NIR light sources. These advantages also allow the integration of pc-NIR-LEDs into smartphones or wearable devices, permitting innovative functional applications. However, developing more efficient NIR phosphors capable of converting the blue LED light to the NIR region is required to advance this technology.

Many ions can generate a broadband NIR emission, such as rare-earth ion Eu $^{2+}$ , and some transition metal ions with 3d configuration. Among them, trivalent chromium has garnered much attention from the research community as an almost ideal NIR emitter due to its high photoluminescence quantum yield (PLQY) as well as a wide excitation range in the blue region and tunable broadband emission when doped into a weak octahedral crystal field environment. As a result, numerous  $Cr^{3+}$ -substituted phosphors have been developed. Unfortunately, the parity-forbidden 3d  $\leftrightarrow$  3d electronic transitions of  $Cr^{3+}$  result in low absorption efficiency (AE), leading to materials with low external quantum efficiency (EQE). For instance,  $Ca_3Sc_2Si_3O_{12}$ :  $Cr^{3+}$  and

 $Gd_3Sc_2Ga_3O_{12}$ : $Cr^{3+}$  have a high PLQY approaching unity, but the low AE (<30%) produces an EQE that is also less than 30%. The EQE is a vital parameter for NIR spectroscopy and therefore needs to be as high as possible to generate sufficient radiant flux and photoelectronic conversion efficiency required for application.  $^{20}$ 

Analyzing possible reasons for the relatively low AE of Cr<sup>3+</sup> activated materials, beyond the intrinsic forbidden electronic transitions, indicatethat many of these materials possess a relatively low Cr<sup>3+</sup> substitution concentration; for example, there is only 0.3 mol % Cr<sup>3+</sup> in Ga<sub>2</sub>O<sub>3</sub>:Cr<sup>3+</sup> and 1.5 mol % Cr<sup>3+</sup> in Ca<sub>3</sub>Sc<sub>2</sub>Si<sub>3</sub>O<sub>12</sub>:Cr<sup>3+</sup> and in Gd<sub>3</sub>Sc<sub>2</sub>Ga<sub>3</sub>O<sub>12</sub>:Cr<sup>3+</sup>. Increasing the Cr<sup>3+</sup> concentration should be a practical approach to enhance AE. This consideration recently helped push the AE to 53.9% in LaMgGa<sub>11</sub>O<sub>19</sub>:Cr<sup>3+</sup> phosphor. The limitation is that higher transition metal concentrations can result in luminescence quenching that decreases the photoluminescence efficiency, meaning AE must be balanced with the photoluminescence quantum yield (PLQY). A more promising approach to increase Cr<sup>3+</sup> absorption is by inducing crystallographic site distortions that break the Laporte rule. Indeed,

Received: October 22, 2021 Revised: December 17, 2021 Published: December 30, 2021





local  ${\rm Cr}^{3+}$  distortions are a practical approach to increase  ${\rm AE}^{26}$  with this idea demonstrated in the  ${\rm Ga}_{2-x}{\rm In}_x{\rm O}_3$ : ${\rm Cr}^{3+}$  phosphor system. Phosphor system. Nevertheless, it remains a challenge to predict which materials will have sufficient symmetry distortion and incorporate a high  ${\rm Cr}^{3+}$  concentration without quenching.

One class of materials where it may be possible to increase the  ${\rm Cr}^{3+}$  substitution concentration is phosphate materials. For example, a recent report showed that 80 mol %  ${\rm Cr}^{3+}$  could be obtained in  ${\rm Sr_9Ga(PO_4)_7:Cr}^{3+}$  (AE = 45%, PLQY = 66.3%), increasing the AE but, more importantly, having a minimal impact on the PLQY. The octahedral substitution sites are significantly separated from one another, which limits concentration quenching. Another advantage of phosphates phosphors is their flexible crystal structures that create a weak crystal field environment around  ${\rm Cr}^{3+}$ , enabling broadband NIR emission with a peak wavelength over 800 nm. Therefore, exploring other phosphate systems is promising for identifying novel broadband NIR phosphor with high AE, resulting in an enhanced PLQY and EQE.

In this work, we investigate a phosphate family with the general formula AMP<sub>2</sub>O<sub>7</sub> (A = Li, Na, K; M = Al, Ga, Sc, In) as a host for Cr<sup>3+</sup>. The monoclinic crystal structure contains nearly octahedral [MO<sub>6</sub>] polyhedra with only slight distortions, making this series an exciting target for efficient NIR photoluminescence. Among the compositions, KGa-P<sub>2</sub>O<sub>7</sub>:Cr<sup>3+</sup> shows the best performance. The similar ionic size between  $Cr^{3+}$  ( $r_{6\text{-coord.}} = 0.615 \text{ Å}$ ) substituting for  $Ga^{3+}$  ( $r_{6\text{-coord.}}$ = 0.62 Å) reduces the likelihood of defect formation and minimizes the propensity for distortions in the crystal structure. The distorted octahedral sites are also wellseparating maximizing Cr3+-Cr3+ separation allowing a comparatively high substitution concentration with minimal concentration quenching. As a result of these structural properties, this phosphor exhibits a broadband emission full width at half-maximum (fwhm = 127 nm,  $\lambda_{em}$  = 815 nm) with a PLQY as high as 74.4% and an AE reaching 44.8% upon 460 nm excitation. Fabricating a NIR pc-LED device further demonstrates that an ultrahigh NIR output power of 473.8 mW and a photoelectric conversion efficiency of 10.7% under 500 mA driven current can be obtained planning this phosphor among the elite materials for NIR spectroscopy applications.

# 2. EXPERIMENTAL SECTION

**2.1. Synthesis.** Samples with the target formula of  $AM_{0.96}Cr_{0.04}P_2O_7$  (A = Li, Na, K; M = Al, Ga, Sc, In) as well as  $KGa_{1-x}Cr_xP_2O_7$  (x = 0, 0.01, 0.02, 0.04, 0.05, 0.8, and 0.1) were synthesized using conventional sintering starting from  $Li_2CO_3$  (Aladdin, 99.99%), NaHCO<sub>3</sub> (Aladdin, 99.99%),  $K_2CO_3$  (Macklin, 99.9%), Al<sub>2</sub>O<sub>3</sub> (Aladdin, 99.99%), Ga<sub>2</sub>O<sub>3</sub> (Aladdin, 99.99%), In<sub>2</sub>O<sub>3</sub> (Aladdin, 99.99%), Sc<sub>2</sub>O<sub>3</sub> (Aladdin, 99.99%), NH<sub>4</sub>H<sub>2</sub>PO<sub>4</sub> (Aladdin, 99.9%), and  $Cr_2O_3$  (Aladdin, 99.99%). First, the starting powders were weighed out in the desired stoichiometric ratios, followed by grinding each sample for 30 min using an agate mortar and pestle. These mixtures were then transferred to alumina crucibles and heated to 850–900 °C in a muffle furnace with a heating rate of 3 °C/min and held for 8–12 h followed by cooling at 3 °C/min. The products were finally cooled to room temperature and ground into a fine powder for subsequent analysis.

**2.2. Characterization.** The phase purity of each sample was checked using powder X-ray diffraction (X'Pert3 PANalytical; Cu  $K\alpha$ ,  $\lambda = 1.5406$  Å) with each diffractogram analyzed using Le Bail or Rietveld refinement. This process was performed within the general structure analysis system (GSAS) software and the EXPGUI interface.<sup>31</sup> The micrographs and elemental distribution of the particles were examined by scanning electron microscopy (SEM)

and energy-dispersive X-ray spectroscopy (EDS)collected on a Hitachi-S4800. The photoluminescence excitation and emission spectra, temperature-dependent emission spectra, and decay curves of the Cr3+-substituted samples were collected on an FLS-980 fluorescence spectrophotometer (Edinburgh Instruments) equipped with a Xenon flash lamp (450 W, Osram). The photoluminescent quantum yields were measured using a Quantaurus-QY Plus C13534-11 (Hamamatsu Photonics), while the diffuse reflectance (DR) spectra were obtained on a UV-vis-NIR spectrophotometer (SHIMADZU, Japan). Both instruments use an integrating sphere with BaSO<sub>4</sub> powder as a standard. The NIR pc-LED device was fabricated by coating a mixture of the as-prepared KGa<sub>0.92</sub>Cr<sub>0.08</sub>P<sub>2</sub>O<sub>7</sub> phosphor and resin with a 1:1 ratio (by weight) on a high-power 450 nm blue LED (Epistar). The electroluminescence spectrum, NIR output power, and photoelectric conversion efficiency of the fabricated NIR pc-LED device as a function of driven current were measured using a HAAS2000 photoelectric measuring system (EVERFINE, China).

**2.3. Computation.** The geometric optimization and electronic property calculations of KGaP<sub>2</sub>O<sub>7</sub> and KGa<sub>0.875</sub>Cr<sub>0.125</sub>P<sub>2</sub>O<sub>7</sub> were performed with the PBE exchange—correlation functional using the Vienna *ab initio* Simulation Package (VASP). These calculations employed a plane-wave pseudopotential total energy package based on density functional theory (DFT). The electronic convergence criteria were set to  $1 \times 10^{-6}$  eV, and the atomic positions and lattice parameters were relaxed to 0.001 eV/Å. The cutoff energy of 500 eV was used for the basis set of the plane waves, and a  $6 \times 4 \times 6$   $\Gamma$ -centered Monkhorst—Pack k-point grid was used to sample the first Brillouin zone.

#### 3. RESULTS AND DISCUSSION

**3.1.** Screening Promising NIR Phosphors from the  $AMP_2O_7$  (A = Li, Na, K; M = Al, Ga, Sc, In) Family. Selecting the optimal combination of elements from the  $AMP_2O_7$  family of phosphors to create the most efficient NIR phosphor was first achieved by experimentally screening the compounds. This required examining a majority of the permutations combining the different A and M elements with a constant substitution concentration of  $Cr^{3+}$  (4 mol %). The combinations of  $AM_{0.96}Cr_{0.04}P_2O_7$ , where A = Li, Na, and K, and M = Al, Ga, Sc, and In, produced pure phase products, as verified by the powder X-ray diffraction (Figure S1), are provided in Figure 1. The photoluminescence excitation

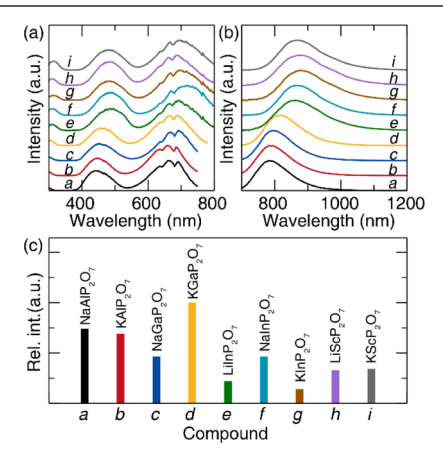


**Figure 1.** (a) Photoluminescent excitation spectra monitored at each emission peak maximum, (b) photoluminescent emission spectra produced when excited by 460 nm blue light, and (c) relative emission peak intensity, in  $AM_{0.96}Cr_{0.04}P_2O_7$  (A = Li, Na, K; M = Al, Ga, Sc, In) family. The corresponding compounds of a—i are provided in (c).

spectra (Figure 1a) indicate that these samples can all be excited by blue-emitting LEDs. Upon 460 nm excitation, a broadband emission, plotted in Figure 1b, is produced covering the 700–1200 nm region. The emission maximum varies depending on the A and M atoms but is generally located between 780 and 900 nm. Comparing the optical properties of the different phosphors shows that the KGaP<sub>2</sub>O<sub>7</sub>:Cr<sup>3+</sup> compound possesses the best overall performance based on the emission peak position, the fwhm, and relative emission peak intensity (Figure 1c). Therefore, a more detailed investigation of the optical properties for KGaP<sub>2</sub>O<sub>7</sub>:Cr<sup>3+</sup> was carried out.

**3.2.** Crystal Structure, Morphology, and Electronic Properties. The quality of the  $KGa_{1-x}Cr_xP_2O_7$  (x=0,0.01,0.02,0.04,0.05,0.8, and 0.1) products was analyzed using powder X-ray diffraction (Figure S2). The resulting diffractograms were completely indexed to the standard  $KGaP_2O_7$  phase (ICSD no. 45007), which belongs to the monoclinic system with a space group of  $P2_1/c$  (no.4).  $Cr^{3+}$  substitution up to 10% does not generate any impurity or average crystal structural distortions. Furthermore, conducting a Rietveld refinement of the X-ray diffractogram for the  $KGa_{0.92}Cr_{0.08}P_2O_7$  sample, as plotted in Figure 2a, shows the

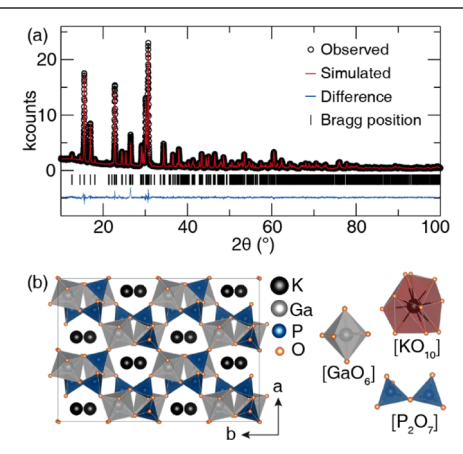


**Figure 2.** (a) Rietveld refinement of the  $KGa_{0.92}Cr_{0.08}P_2O_7$  sample; (b) crystal structure of  $KGaP_2O_7$  shown as a  $2 \times 2 \times 2$  supercell. The coordination environments for each cation are shown.

sample has excellent phase purity and that the crystal structure agrees with the previously published data. The refined results and atom positions are listed in Tables 1 and S1. The best way

Table 1. Refined Results from the KGa<sub>0.92</sub>Cr<sub>0.08</sub>P<sub>2</sub>O<sub>7</sub> X-ray Powder Diffractograms

formula	$KGa_{0.92}Cr_{0.08}P_2O_7$
radiation type; $\lambda$ (Å)	X-ray; 1.5406
$2\theta$ range (deg)	10-100
temperature (°C)	25
space group; Z	$P2_1/c; 2$
a (Å)	7.3240(1)
b (Å)	9.8287(1)
c (Å)	8.15137(2)
$\beta$ (deg)	106.71(5)
unit cell volume (Å3)	562.0(1)
profile R-factor, $R_{\rm p}$	0.0487
weighted profile R-factor, $R_{\rm wp}$	0.0665
$\chi^2$	4.23

to view KGaP<sub>2</sub>O<sub>7</sub> is by drawing a 2 × 2 × 2 supercell, as illustrated in Figure 2b. As shown, the crystal structure is composed of [KO<sub>10</sub>], [GaO<sub>6</sub>], and [P<sub>2</sub>O<sub>7</sub>] units, forming a rigid three-dimensional framework. Only the octahedral Ga<sup>3+</sup> ( $r_{6\text{-coord.}} = 0.62 \text{ Å}$ ) site is available for Cr<sup>3+</sup> ( $r_{6\text{-coord.}} = 0.615 \text{ Å}$ ) to occupy due to their similar ionic size,<sup>36</sup> which was also confirmed by structural refinement. As depicted, the [GaO<sub>6</sub>] octahedral units are slightly distorted from perfect octahedral symmetry, having refined Ga–O bond lengths of 1.93–1.98 Å and bond Ga–O bond angles of 83.5–98.3°. It is possible to quantify the magnitude of the distortion by calculating the distortion index (D) using eq 1<sup>37,38</sup>

$$D = \frac{1}{n} \sum_{i=1}^{n} \frac{|l_i - l_{av}|}{l_{av}}$$
 (1)

where  $l_i$  represents the bond length separating the central atom from the ith coordinating atom, and  $l_{\rm av}$  is the average bond length. The calculated D for the AMP $_2$ O $_7$  (A = Li, Na, K; M = Al, Ga, Sc, In) family, provided as Figure S3, demonstrates that KGaP $_2$ O $_7$  has the lowest site distortion index (D = 0.00755) among those compounds. This subtle distortion is crucial because it suggests that  $Cr^{3+}$  substitution in KGaP $_2$ O $_7$  will have optical properties representative of a transition metal in an octahedral environment while having an improved AE because Laporte's rule is broken. The individual octahedral units are also separated by >5 Å allowing a high  $Cr^{3+}$  concentration with minimal quenching expected.

The morphology of the KGa<sub>0.92</sub>Cr<sub>0.08</sub>P<sub>2</sub>O<sub>7</sub> sample was examined by SEM, as shown in Figure 3a. The particles

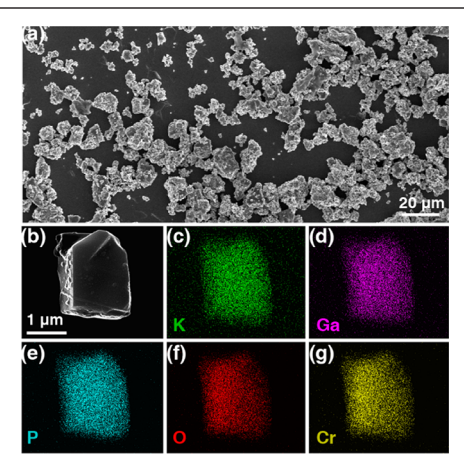


Figure 3. (a) Scanning electron micrographs (SEM) collected using secondary electrons and (b–g) EDS mapping on the surface of the  $KGa_{0.92}Cr_{0.08}P_2O_7$  sample.

generally show an irregular shape with an estimated diameter of  $5-10~\mu m$ . Using EDS to map the elemental distribution on a randomly selected single particle verifies that only the loaded elements K, Ga, P, O, and Cr can be detected. The distribution of all these elements also appears to be uniform throughout the sample (Figure 3b-g).

The electronic band structures of the pristine and  $Cr^{3+}$  substituted compounds were calculated using the GGA-PBE functional. The density of states of KGaP<sub>2</sub>O<sub>7</sub> is presented in Figure 4a, and the band structure is shown in Figure S4. KGaP<sub>2</sub>O<sub>7</sub> shows an indirect electronic transition (B  $\rightarrow$   $\Gamma$ ) with a calculated band ( $E_{\rm g,PBE}$ ) of 4.32 eV. This value is consistent with the measured optical band gap ( $E_{\rm g,optical}$  = 4.39 eV)

**Chemistry of Materials** Article pubs.acs.org/cm

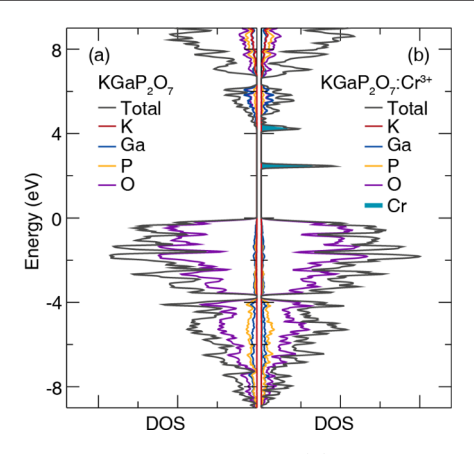


Figure 4. Density of states of (a) KGaP2O7 and (b) KGa<sub>0.875</sub>Cr<sub>0.125</sub>P<sub>2</sub>O<sub>7</sub> calculated using the PBE functional.

obtained from the Kubelka-Munk transformed absorption spectrum (Figure S5).<sup>39</sup> The band gap is set by the O 2p states as the valence band and the Ga 3d states as the conduction band. The emergence of Cr 3d states can be observed within the band gap when calculating a hypothetical KGaP<sub>2</sub>O<sub>7</sub> substituted with 12.5 mol % Cr<sup>3+</sup>, as illustrated in Figure 4b. The Cr 3d states are split with two of the 3d orbitals falling near the conduction band and the remaining three 3d orbitals in the middle of the band gap following the nearly octahedral coordination environment. The interpretation of the Cr<sup>3+</sup> states at the GGA-PBE level of theory, although semiqualitative in nature, provides essential information regarding the transition metal orbital positions in the host structure band gap and offers hints for this material's phosphor performance.

3.3. Photoluminescence. The diffuse reflectance spectrum and photoluminescence spectrum of a selected KGa<sub>0.92</sub>Cr<sub>0.08</sub>P<sub>2</sub>O<sub>7</sub> sample are shown in Figure 5. The DR spectrum (Figure 5a, dashed line) has three absorption peaks in the ultraviolet (300 nm), blue (457 nm), and red (662 nm) regions. Considering the nearly octahedral coordination of Cr<sup>3+</sup>, these transitions correspond closely to the respective

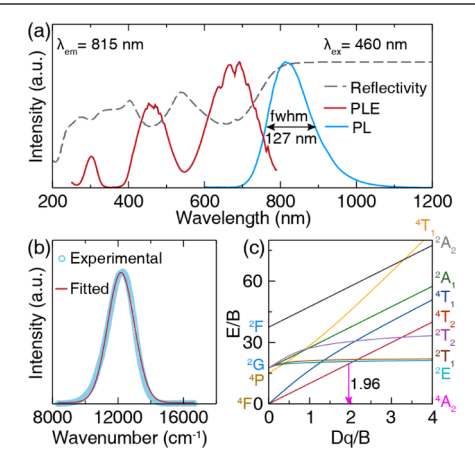


Figure 5. (a) Diffuse reflectance (gray dashed line), photoluminescence excitation spectrum (red line), and photoluminescence emission spectrum (blue line) of KGa<sub>0.92</sub>Cr<sub>0.08</sub>P<sub>2</sub>O<sub>7</sub>. (b) Single Gaussian function describes the emission spectrum of KGa<sub>0.92</sub>Cr<sub>0.08</sub>P<sub>2</sub>O<sub>7</sub>. (c) Cr<sup>3+</sup> in a nearly octahedral environment can be approximated using the Tanabe-Sugano diagram for octahedral crystal field splitting. This analysis indicates that the transition metal in KGa<sub>0.92</sub>Cr<sub>0.08</sub>P<sub>2</sub>O<sub>7</sub> experiences a weak crystal field environment.

transitions of  $^4A_2 \rightarrow {}^4T_1$  ( $^4P$ ),  $^4A_2 \rightarrow {}^4T_1$  ( $^4F$ ), and  $^4A_2 \rightarrow {}^4T_2$  ( $^4F$ ) in the nominally  $O_h$  environment. These transitions are consistent with the excitation spectrum monitored at 815 nm, which is plotted as the red line in Figure 5. Exciting the sample with 460 nm light causes an intense broadband emission covering 700-1100 nm, with the peak centered at 815 nm. The fwhm of the peak is 127 nm (1874 cm $^{-1}$ ). The emission spectrum is straightforwardly described by a single Gaussian peak (Figure 5b), signifying that only one crystallographically independent emission center is present in this compound. Because the Cr<sup>3+</sup> coordination environment is nearly octahedral, the crystal field strength can thus be approximated based on the crystal field splitting  $(D_a)$  and the Racah parameter (B), which is calculated by following eqs 2-4.42

$$10D_{q} = E(^{4}T_{2}) = E(^{4}A_{2} \to {}^{4}T_{2})$$
(2)

$$\frac{D_{\rm q}}{B} = \frac{15(x-8)}{x^2 - 10x} \tag{3}$$

$$x = \frac{E(^{4}A_{2} \to {}^{4}T_{1}) - E(^{4}A_{2} \to {}^{4}T_{2})}{D_{q}}$$
(4)

The  $D_{q}$  and B parameters were calculated to be 1474.9 and 751.8 cm<sup> $^{4}$ </sup> resulting in a  $D_{q}/B$  of 1.96 (Figure 5c). This phosphate, therefore, exhibits a relatively weak crystal field environment on the  $Cr^{3+}$  luminescence center as desired. Further varying the  $Cr^{3+}$  concentration from 1 to 10 mol %

indicates that the excitation spectra (Figure 6a) are nearly

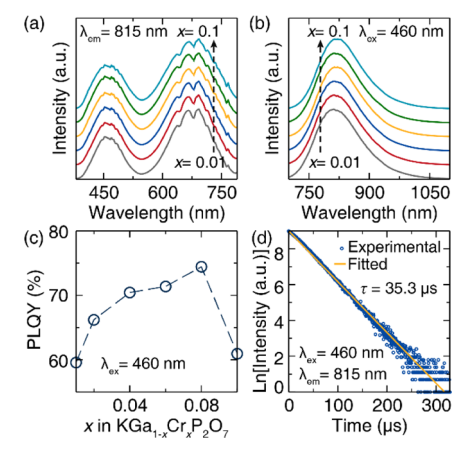


Figure 6. (a) Photoluminescence excitation spectra monitored at 815 nm and (b) photoluminescence emission spectra excited by 460 nm of  $KGa_{1-x}Cr_xP_2O_7$  (x = 0.01, 0.02, 0.04, 0.06, 0.08, and 0.1) phosphor; (c) PLQY as a function of  $Cr^{3+}$  concentration x in  $KGa_{1-x}Cr_xP_2O_7$  (x = 0.01, 0.02, 0.04, 0.06, 0.08, and 0.1) phosphor; (d) room-temperature decay curve of  $KGa_{0.92}Cr_{0.08}P_2O_7$  ( $\lambda_{ex}$  = 460 nm,  $\lambda_{\rm em}$  = 815 nm), and fit by a monoexponential function.

unchanged, suggesting the crystal field splitting is not influenced by the amount of Cr3+. However, the emission spectra (Figure 6b) display a slight red-shift (~3 nm) and an unusual narrowing (~5 nm), which is mainly ascribed to strong reabsorption caused by the overlapping excitation and emission spectra. The optimal Cr3+ concentration was found based on the PLQY to occur in the 8 mol % sample (Figure 6c), beyond which concentration quenching occurs. Although this does not seem like a significant substitution percentage,

this value is higher than most reported  $Cr^{3+}$ -activated materials. There is only 4 mol % in  $LiScP_2O_7:Cr^{3+}$ , 0.3 mol % in  $Ga_2O_3:Cr^{3+}$ , and 6 mol % in  $LiInSi_2O_6:Cr^{3+}:^{23,29,43}$  Under 460 nm excitation, the PLQY of  $KGa_{0.92}Cr_{0.08}P_2O_7$  reaches 74.4% (Figure S6), making the internal quantum yield higher than  $LiScP_2O_7:Cr^{3+}$  (38%) and  $Sr_9Ga\left(PO_4\right)_7:Cr^{3+}$  (66.3%). It is also competitive with the most efficient reported  $Cr^{3+}$  phosphor,  $LiInSi_2O_6:Cr^{3+}$  (75%). The AE was also surprisingly high (44.8%), placing this material among the best-reported  $Cr^{3+}$  phosphors that have both high PLQY and AE values. As a result, the EQE reaches as high as 33.3%.

The room-temperature photoluminescence decay curve of  $KGa_{0.92}Cr_{0.08}P_2O_7$  was also collected using a 460 nm excitation source and monitored at 815 nm (Figure 6d). A monoexponential function was found to describe the lifetime yielding a  $\tau=35.3~\mu s$ . This is surprisingly short compared to most reported  $Cr^{3+}$ -substituted materials, such as  $Ga_2O_3:Cr^{3+}$  (230.1  $\mu s$ ),  $Sr_9Ga(PO_4)_7:Cr^{3+}$  (111.0  $\mu s$ ),  $LiInSi_2O_6:Cr^{3+}$  (43.2  $\mu s$ ), and  $Ca_3Sc_2Si_3O_{12}:Cr^{3+}$  (80.5  $\mu s$ ).  $^{21,23,28,43}$  The fast decay is permitted by the low site symmetry breaking the forbidden nature of the electronic transition. A short relaxation time is advantageous because it indicates that the material will be less prone to excitation saturation effects, which can lower the phosphor's photoluminescence efficiency when the pump LED is driven by very high current.

**3.4.** Temperature-Dependent Emission Properties. Thermal stability is another critical factor that must be considered for any practical application of NIR luminescent materials. The efficiency and emission peak position must remain constant even at elevated temperatures. Thus, the temperature-dependent emission spectrum of  $KGa_{0.92}Cr_{0.08}P_2O_7$  was collected from 298 to 473 K (Figure S7a). The contour plot of the temperature-dependent photoluminescence spectra and normalized integrated (peak) intensity are depicted in Figure 7a,b, respectively. As shown, the emission intensity gradually decreases with increasing temperature. The material retains 56.0% of the initial intensity at 423 K. This is higher than comparable  $Cr^{3+}$  phosphate phosphors, such as  $Sr_8MgLa(PO_4)_7$ : $Cr^{3+}$  (<10%),  $Sr_9Ga-(PO_4)_7$ : $Cr^{3+}$  (<10%), and  $LiScP_2O_7$ : $Cr^{3+}$  (<20%),  $Cr^{3+}$  dem-

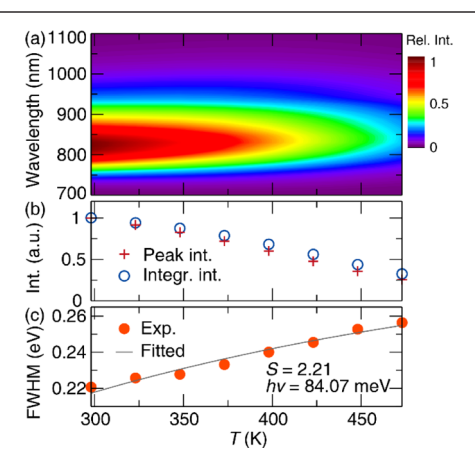


Figure 7. (a) Contour plot of the temperature-dependent photoluminescence emission spectra of the  $KGa_{0.92}Cr_{0.08}P_2O_7$  phosphor excited by 460 nm; (b) normalized integrated intensity and peak intensity of the photoluminescence emission spectra as a function of temperature in the region of 298–473 K; (c) calculated Huang–Rhys factor (S) and phonon energy (hv) as a function of temperature in the  $KGa_{0.92}Cr_{0.08}P_2O_7$  phosphor.

onstrating the superior thermal stability of this material. <sup>28–30</sup> Moreover, the normalized emission spectrum (Figure S7b,c) demonstrates a gradual but minor broadening and redshift of emission spectra as the increase of temperature. These changes are due to weaker crystal field splitting around the Cr<sup>3+</sup> luminescence center. The concurrent broadening of the emission peak's fwhm stems from increasing electron—phonon coupling at elevated temperatures.

The thermal stability of  $KGa_{0.92}Cr_{0.08}P_2O_7$  is generally related to the degree of electron—phonon coupling, which can be characterized by Huang—Rhys factor (S). The best approach to determine S is by fitting the temperature-dependent photoluminescence following eq  $5^{45}$ 

$$FWHM(T) = \sqrt{8 \ln 2} \times h\nu \times \sqrt{\coth(h\nu/2kT)}$$
 (5)

where the fwhm (eV) is the full width at half-maximum obtained from fitting each emission spectra at temperature T (K), hv is the phonon energy, and k is Boltzmann's constant. Analyzing the relationship between fwhm and T with this equation provides the results, as shown in Figure 7c. Here, S and hv were determined to be 2.21 and 80.07 meV, respectively. These values are consistent with the empirical equation  $S = (1/2E_{\rm Stokes}/\hbar\omega + 1/4) \pm 1/4$  (Figure S8), validating the accuracy. Compared to other reported broadband NIR phosphors, the Huang–Rhys S value of  $KGa_{0.92}Cr_{0.08}P_2O_7$  is much lower, demonstrating weak electron–phonon coupling in this compound.

The thermal quenching mechanism can also be analyzed by calculating the thermal quenching activation energy ( $\Delta E$ ) based on eq  $6^{46,47}$ 

$$I_{\rm T} = \frac{I_0}{1 + A \, \exp\left(\frac{-\Delta E}{kT}\right)} \tag{6}$$

where  $I_T$  represents the emission intensity at temperature T(K),  $I_0$  refers to the initial emission intensity, k stands for the Boltzmann's constant, A is a constant related to host material, and  $\Delta E$  is the activation energy of thermal quenching. Rearranging the equation and plotting  $ln(I_0/I_T - 1)$  against 1/kT (Figure S9) shows the data can be fit linearly with a high degree of confidence ( $R^2 = 0.998$ ). The  $\Delta E$  from this analysis was subsequently estimated to be 0.30 eV (A = 3983.8), which is higher than that in  $Sr_9Ga(PO_4)_7$ : $Cr^{3+}$  (0.19 eV),<sup>28</sup> demonstrating a relatively high energy barrier to resist thermal quenching in KGa<sub>0.92</sub>Cr<sub>0.08</sub>P<sub>2</sub>O<sub>7</sub>. Considering the separation of the conduction band and the Cr3+ 3d orbitals is relatively narrow, as determined in the electronic band structure (Figure S4b), increasing the band gap could be a viable route to improve the temperature-dependent photoluminescence of this phosphor.

**3.5.** Application to NIR pc-LEDs. A prototype high-power NIR pc-LED device was constructed to evaluate the practical application performance by combining the as-synthesized KGa<sub>0.92</sub>Cr<sub>0.08</sub>P<sub>2</sub>O<sub>7</sub> phosphor with a 450 nm blue InGaN chip. The resulting device is shown in the insets of Figure 8a. As presented, the body color of this phosphor is deep green indicating the significant absorption of blue and red photons. Figure 8a shows the electroluminescence spectra of the NIR pc-LED device obtained at various forward bias currents, ranging from 50 to 500 mA. The NIR output power and NIR photoelectric conversion efficiency increase, as plotted in Figure 8b, without saturating from 57.5 to 473.8 mW. Thus, this material shows minimal excitation saturation effects,

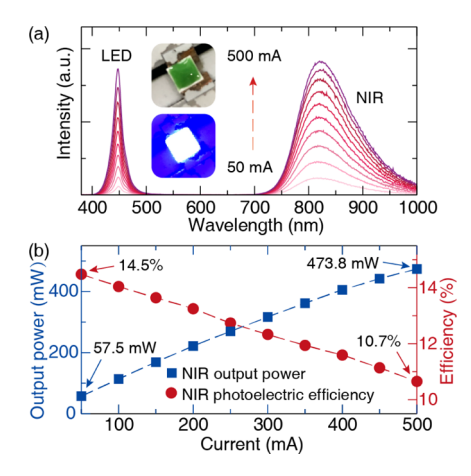


**Figure 8.** Electroluminescence spectra of the prototype pc-NIR-LED plotted as a function of the driving current. The insets show photographs of the NIR pc-LED off (top) and on (bottom). (b) NIR output power and photoelectric conversion efficiency of pc-NIR-LED.

making it optimal for high-power applications. The NIR photoelectronic conversion efficiency gradually decreases from 14.5 to 10.7%, indicating that this device's energy conversion efficiency mainly stems from the excellent EQE of the phosphor. Notably, the NIR output power reaches 473.8 mW and with a NIR photoelectric efficiency of 10.7% when driven at 500 mA. This surpasses the best high-power NIR LED device currently reported (467 mW@10.4% under a current of 500 mA) that uses the  $Gd_3Sc_2Ga_3O_{12}:Cr^{3+}$  phosphor. These results demonstrate that  $KGaP_2O_7:Cr^{3+}$  phosphor has excellent potential as a key material for high-power broadband NIR pc-LEDs applications.

#### 4. CONCLUSIONS

In summary, a series of phosphate-based phosphors were screened for efficient NIR broadband photon emission. The best material identified from this study was found to be KGaP<sub>2</sub>O<sub>7</sub>:Cr<sup>3+</sup>, which strongly absorbs blue LED as exemplified by the green body color of the phosphor and produces an intense emission centered at 815 nm emission with a fwhm of 127 nm and a high PLQY (74.4%), enabling an EQE as high as 33.3%. Studying the temperature-dependent photoluminescence shows that 56.0% of the room temperature emission intensity is maintained at 423 K owing to the relatively weak phonon-electron coupling as supported by the material's low Huang-Rhys value (S = 2.21). Finally, a prototype NIR pc-LED device fabricated by using the asprepared phosphor combined with a high-power 450 nm blue LED presents ultrahigh NIR output power and excellent NIR photoelectric conversion efficiency (473.8 mW@10.7%, under driving current of 500 mA), demonstrating a great potential of KGaP<sub>2</sub>O<sub>7</sub>:Cr<sup>3+</sup> phosphor as a key material for applications in high-power NIR pc-LEDs.

#### ASSOCIATED CONTENT

#### Supporting Information

The Supporting Information is available free of charge at https://pubs.acs.org/doi/10.1021/acs.chemmater.1c03671.

Powder XRD, distortion index, electronic band structures, DR spectra, optical band gap, PLQY, normalized temperature-dependent emission spectra, thermal quenching activation energy, and atom position (PDF)

#### AUTHOR INFORMATION

# **Corresponding Authors**

Weiren Zhao — School of Physics and Optoelectronic Engineering, Guangdong University of Technology, Guangzhou 510006, China; Email: zwren123@126.com Jakoah Brgoch — Department of Chemistry, University of

Houston, Houston, Texas 77204, United States;
o orcid.org/0000-0002-1406-1352; Email: jbrgoch@uh.edu

#### **Authors**

Jiyou Zhong — School of Physics and Optoelectronic Engineering, Guangdong University of Technology, Guangzhou 510006, China; orcid.org/0000-0003-2817-6617

Chaojie Li – School of Physics and Optoelectronic Engineering, Guangdong University of Technology, Guangzhou 510006, China

Shihai You — College of Materials, Xiamen University, Xiamen 361005, China; orcid.org/0000-0002-1537-7148

Complete contact information is available at: https://pubs.acs.org/10.1021/acs.chemmater.1c03671

#### Notes

The authors declare no competing financial interest.

# ACKNOWLEDGMENTS

The authors thank the National Natural Science Foundation of China (no. 51702057) and the National Science Foundation (DMR-1847701).

#### REFERENCES

- (1) Lucero, A. A.; Addae, G.; Lawrence, W.; Neway, B.; Credeur, D. P.; Faulkner, J.; Rowlands, D.; Stoner, L. Reliability of Muscle Blood Flow and Oxygen Consumption Response from Exercise Using Near-Infrared Spectroscopy. *Exp. Physiol.* **2018**, *103*, 90–100.
- (2) Magwaza, L. S.; Opara, U. L.; Nieuwoudt, H.; Cronje, P. J. R.; Saeys, W.; Nicolaï, B. NIR Spectroscopy Applications for Internal and External Quality Analysis of Citrus Fruit-A Review. *Food Bioprocess Technol.* **2012**, *5*, 425–444.
- (3) Scholkmann, F.; Kleiser, S.; Metz, A. J.; Zimmermann, R.; Mata Pavia, J.; Wolf, U.; Wolf, M. A Review on Continuous Wave Functional Near-Infrared Spectroscopy and Imaging Instrumentation and Methodology. *Neuroimage* **2014**, *85*, 6–27.
- (4) Grassi, B.; Quaresima, V. Near-infrared spectroscopy and skeletal muscle oxidative function vivoin health and disease: a review from an exercise physiology perspective. *J. Biomed. Opt.* **2016**, *21*, 091313.
- (5) Rajendran, V.; Fang, M.-H.; Guzman, G. N. D.; Lesniewski, T.; Mahlik, S.; Grinberg, M.; Leniec, G.; Kaczmarek, S. M.; Lin, Y.-S.; Lu, K.-M.; Lin, C.-M.; Chang, H.; Hu, S.-F.; Liu, R.-S. Super Broadband Near-Infrared Phosphors with High Radiant Flux as Future Light Sources for Spectroscopy Applications. *ACS Energy Lett.* **2018**, 3, 2679–2684.
- (6) Fang, M.-H.; Huang, P.-Y.; Bao, Z.; Majewska, N.; Leśniewski, T.; Mahlik, S.; Grinberg, M.; Leniec, G.; Kaczmarek, S. M.; Yang, C.-W.; Lu, K.-M.; Sheu, H.-S.; Liu, R.-S. Penetrating Biological Tissue Using Light-Emitting Diodes with a Highly Efficient Near-Infrared ScBO<sub>3</sub>:Cr<sup>3+</sup> Phosphor. *Chem. Mater.* **2020**, 32, 2166–2171.
- (7) Huang, W.-T.; Cheng, C.-L.; Bao, Z.; Yang, C.-W.; Lu, K.-M.; Kang, C.-Y.; Lin, C.-M.; Liu, R.-S. Broadband Cr<sup>3+</sup>, Sn<sup>4+</sup>-doped Oxide Nanophosphors for Infrared Mini Light-Emitting Diodes. *Angew. Chem.* **2018**, *131*, 2091.

- (8) Xie, R.-J. Light-Emitting Diodes: Brighter NIR-Emitting Phosphor Making Light Sources Smarter. *Light Sci. Appl.* **2020**, *9*, 9–10.
- (9) He, S.; Zhang, L.; Wu, H.; Wu, H.; Pan, G.; Hao, Z.; Zhang, X.; Zhang, L.; Zhang, H.; Zhang, J. Efficient Super Broadband NIR Ca<sub>2</sub>LuZr<sub>2</sub>Al<sub>3</sub>O<sub>12</sub>:Cr<sup>3+</sup>, Yb<sup>3+</sup> Garnet Phosphor for pc-LED Light Source toward NIR Spectroscopy Applications. *Adv. Opt. Mater.* **2020**, *8*, 1901684.
- (10) Liu, G.; Hu, T.; Molokeev, M. S.; Xia, Z. Li/Na Substitution and Yb<sup>3+</sup> Co-Doping Enabling Tunable near-Infrared Emission in LiIn<sub>2</sub>SbO<sub>6</sub>:Cr<sup>3+</sup> Phosphors for Light-Emitting Diodes. *iScience* **2021**, 24, 102250.
- (11) Qiao, J.; Zhou, G.; Zhou, Y.; Zhang, Q.; Xia, Z. Divalent Europium-Doped near-Infrared-Emitting Phosphor for Light-Emitting Diodes. *Nat. Commun.* **2019**, *10*, 5267.
- (12) Tang, Z.; Zhang, Q.; Cao, Y.; Li, Y.; Wang, Y. Eu<sup>2+</sup>-Doped Ultra-Broadband VIS-NIR Emitting Phosphor. *Chem. Eng. J.* **2020**, 388, 124231.
- (13) Yang, Z.; Zhao, Y.; Zhou, Y.; Qiao, J.; Chuang, Y.-C.; Molokeev, M. S.; Xia, Z. Giant Red-Shifted Emission in (Sr,Ba)-Y<sub>2</sub>O<sub>4</sub>:Eu<sup>2+</sup> Phosphor Toward Broadband Near-Infrared Luminescence. *Adv. Funct. Mater.* **2021**, 2103927.
- (14) Joos, J. J.; Van der Heggen, D.; Martin, L. I. D. J.; Amidani, L.; Smet, P. F.; Barandiarán, Z.; Seijo, L. Broadband Infrared LEDs Based on Europium-to-Terbium Charge Transfer Luminescence. *Nat. Commun.* **2020**, *11*, 1–11.
- (15) Wei, Y.; Dang, P.; Dai, Z.; Li, G.; Lin, J. Advances in Near-Infrared Luminescent Materials without Cr<sup>3+</sup>: Crystal Structure Design, Luminescence Properties, and Applications. *Chem. Mater.* **2021**, *33*, 5496–5526.
- (16) Song, E.; Ming, H.; Zhou, Y.; He, F.; Wu, J.; Xia, Z.; Zhang, Q. Cr<sup>3+</sup>-Doped Sc-Based Fluoride Enabling Highly Efficient Near Infrared Luminescence: A Case Study of K<sub>2</sub>NaScF<sub>6</sub>:Cr3+. *Laser Photon. Rev.* **2021**, *15*, 2000410.
- (17) Gao, T.; Zhuang, W.; Liu, R.; Liu, Y.; Yan, C.; Chen, X. Design of a Broadband NIR Phosphor for Security-Monitoring LEDs: Tunable Photoluminescence Properties and Enhanced Thermal Stability. *Cryst. Growth Des.* **2020**, *20*, 3851–3860.
- (18) De Guzman, G. N. A.; Hu, S. F.; Liu, R. S. Enticing applications of near-infrared phosphors: Review and future perspectives. *J. Chin. Chem. Soc.* **2021**, *68*, 206–215.
- (19) De Guzman, G. N. A.; Fang, M.-H.; Liang, C.-H.; Bao, Z.; Hu, S.-F.; Liu, R.-S. Near-infrared phosphors and their full potential: A review on practical applications and future perspectives. *J. Lumin.* **2020**, *219*, 116944.
- (20) He, F.; Song, E.; Zhou, Y.; Ming, H.; Chen, Z.; Wu, J.; Shao, P.; Yang, X.; Xia, Z.; Zhang, Q. A General Ammonium Salt Assisted Synthesis Strategy for Cr<sup>3+</sup>-Doped Hexafluorides with Highly Efficient Near Infrared Emissions. *Adv. Funct. Mater.* **2021**, *31*, 2103743.
- (21) Jia, Z.; Yuan, C.; Liu, Y.; Wang, X.-J.; Sun, P.; Wang, L.; Jiang, H.; Jiang, J. Strategies to Approach High Performance in Cr<sup>3+</sup>-Doped Phosphors for High-Power NIR-LED Light Sources. *Light Sci. Appl.* **2020**, *9*, 86.
- (22) Basore, E. T.; Xiao, W.; Liu, X.; Wu, J.; Qiu, J. Broadband Near-Infrared Garnet Phosphors with Near-Unity Internal Quantum Efficiency. *Adv. Opt. Mater.* **2020**, *8*, 2000296.
- (23) Fang, M.-H.; De Guzman, G. N. A.; Bao, Z.; Majewska, N.; Mahlik, S.; Grinberg, M.; Leniec, G.; Kaczmarek, S. M.; Yang, C.-W.; Lu, K.-M.; Sheu, H.-S.; Hu, S.-F.; Liu, R.-S. Ultra-high-efficiency nearinfrared Ga<sub>2</sub>O<sub>3</sub>:Cr<sup>3+</sup> phosphor and controlling of phytochrome. *J. Mater. Chem. C* **2020**, *8*, 11013–11017.
- (24) Fang, M.-H.; Chen, K.-C.; Majewska, N.; Leśniewski, T.; Mahlik, S.; Leniec, G.; Kaczmarek, S. M.; Yang, C.-W.; Lu, K.-M.; Sheu, H.-S.; Liu, R.-S. Hidden Structural Evolution and Bond Valence Control in Near-Infrared Phosphors for Light-Emitting Diodes. *ACS Energy Lett.* **2021**, *6*, 109–114.
- (25) Liu, S.; Wang, Z.; Cai, H.; Song, Z.; Liu, Q. Highly efficient near-infrared phosphor LaMgGa<sub>11</sub>O<sub>19</sub>:Cr<sup>3+</sup>. *Inorg. Chem. Front.* **2020**, 7, 1467–1473.

- (26) Grinberg, M.; Jaskolski, W.; Macfarlane, P. I.; Henderson, B.; Holliday, K. Crystal Field Distribution and Non-Radiative Transitions in Cr<sup>3+</sup>-Doped Gallogermanates. *J. Lumin.* **1997**, 72–74, 193–194.
- (27) Zhong, J.; Zhuo, Y.; Du, F.; Zhang, H.; Zhao, W.; Brgoch, J. Efficient and Tunable Luminescence in Ga<sub>2-x</sub>In<sub>x</sub>O<sub>3</sub>:Cr<sup>3+</sup> for Near-Infrared Imaging. ACS Appl. Mater. Interfaces **2021**, *13*, 31835–31842.
- (28) Zhao, F.; Cai, H.; Song, Z.; Liu, Q. Structural Confinement for Cr<sup>3+</sup> Activators toward Efficient Near-Infrared Phosphors with Suppressed Concentration Quenching. *Chem. Mater.* **2021**, 33, 3621–3630.
- (29) Yao, L.; Shao, Q.; Han, S.; Liang, C.; He, J.; Jiang, J. Enhancing Near-Infrared Photoluminescence Intensity and Spectral Properties in Yb<sup>3+</sup> Codoped LiScP<sub>2</sub>O<sub>7</sub>:Cr<sup>3+</sup>. *Chem. Mater.* **2020**, 32, 2430–2439.
- (30) Malysa, B.; Meijerink, A.; Jüstel, T. Temperature Dependent Photoluminescence of  $Cr^{3+}$  Doped  $Sr_8MgLa(PO_4)_7$ . Opt. Mater. **2018**, 85, 341–348.
- (31) Toby, B. H. EXPGUI, a graphical user interface for GSAS. J. Appl. Crystallogr. 2001, 34, 210–213.
- (32) Hafner, J. Ab-initiosimulations of materials using VASP: Density-functional theory and beyond. *J. Comput. Chem.* **2008**, 29, 2044–2078.
- (33) Kresse, G.; Furthmüller, J. Efficient iterative schemes forab initiototal-energy calculations using a plane-wave basis set. *Phys. Rev. B: Condens. Matter Mater. Phys.* **1996**, *54*, 11169–11186.
- (34) Kresse, G.; Hafner, J. Ab initiomolecular dynamics for liquid metals. *Phys. Rev. B: Condens. Matter Mater. Phys.* **1993**, 47, 558–561.
- (35) Hohenberg, P.; Kohn, W. Inhomogeneous Electron Gas. *Phys. Rev.* **1964**, *136*, B864–B871.
- (36) Shannon, R. D. Revised Effective Ionic Radii and Systematic Studies of Interatomic Distances in Halides and Chalcogenides. *Acta Crystallogr., Sect. A: Cryst. Phys., Diffr., Theor. Gen. Crystallogr.* 1976, 32, 751–767.
- (37) Baur, W. H. The Geometry of Polyhedral Distortions. Predictive Relationships for the Phosphate Group. *Acta Crystallogr., Sect. B: Struct. Sci., Cryst. Eng. Mater.* **1974**, 30, 1195–1215.
- (38) Zhong, J.; Zhao, W.; Zhuang, W.; Xiao, W.; Zheng, Y.; Du, F.; Wang, L. Origin of Spectral Blue Shift of Lu<sup>3+</sup>-Codoped YAG:Ce<sup>3+</sup> Phosphor: First-Principles Study. *ACS Omega* **2017**, *2*, 5935–5941.
- (39) Makuła, P.; Pacia, M.; Macyk, W. How To Correctly Determine the Band Gap Energy of Modified Semiconductor Photocatalysts Based on UV-Vis Spectra. *J. Phys. Chem. Lett.* **2018**, *9*, 6814–6817.
- (40) Bai, B.; Dang, P.; Huang, D.; Lian, H.; Lin, J. Broadband Near-Infrared Emitting Ca<sub>2</sub>LuScGa<sub>2</sub>Ge<sub>2</sub>O<sub>12</sub>:Cr<sup>3+</sup> Phosphors: Luminescence Properties and Application in Light-Emitting Diodes. *Inorg. Chem.* **2020**, *59*, 13481–13488.
- (41) Liu, G.; Molokeev, M. S.; Lei, B.; Xia, Z. Two-site  $Cr^{3+}$  occupation in the  $MgTa_2O_6$ : $Cr^{3+}$  phosphor toward broad-band near-infrared emission for vessel visualization. *J. Mater. Chem. C* **2020**, 8, 9322–9328.
- (42) Struve, B.; Huber, G. The Effect of the Crystal Field Strength on the Optical Spectra of Cr<sup>3+</sup> in Gallium Garnet Laser Crystals. *Appl. Phys. B: Photophys. Laser Chem.* **1985**, *36*, 195–201.
- (43) Xu, X.; Shao, Q.; Yao, L.; Dong, Y.; Jiang, J. Highly Efficient and Thermally Stable Cr<sup>3+</sup>-Activated Silicate Phosphors for Broadband near-Infrared LED Applications. *Chem. Eng. J.* **2020**, 383, 123108.
- (44) Lin, Q.; Wang, Q.; Liao, M.; Xiong, M.; Feng, X.; Zhang, X.; Dong, H.; Zhu, D.; Wu, F.; Mu, Z. Trivalent Chromium Ions Doped Fluorides with Both Broad Emission Bandwidth and Excellent Luminescence Thermal Stability. *ACS Appl. Mater. Interfaces* **2021**, 13, 18274–18282.
- (45) Liu, C.; Qi, Z.; Ma, C.-G.; Dorenbos, P.; Hou, D.; Zhang, S.; Kuang, X.; Zhang, J.; Liang, H. High Light Yield of  $Sr_8(Si_4O_{12})$ - $Cl_8$ :Eu<sup>2+</sup> under X-Ray Excitation and Its Temperature-Dependent Luminescence Characteristics. *Chem. Mater.* **2014**, *26*, 3709–3715.
- (46) Xia, Z.; Liu, R.-S. Tunable Blue-Green Color Emission and Energy Transfer of Ca<sub>2</sub>Al<sub>3</sub>O<sub>6</sub>F:Ce<sup>3+</sup>,Tb<sup>3+</sup> Phosphors for Near-UV White LEDs. *J. Phys. Chem. C* **2012**, *116*, 15604–15609.

(47) Zhong, J.; Zhuang, W.; Xing, X.; Liu, R.; Li, Y.; Liu, Y.; Hu, Y. Synthesis, Crystal Structures, and Photoluminescence Properties of Ce<sup>3+</sup>-Doped Ca<sub>2</sub>LaZr<sub>2</sub>Ga<sub>3</sub>O<sub>12</sub>: New Garnet Green-Emitting Phosphors for White Leds. *J. Phys. Chem. C* **2015**, *119*, 5562–5569.

